

AD-A229 856

RADC-TR-90-234
Final Technical Report
September 1990



DIRECT OPTICAL TO MICROWAVE CONVERSION

Texas A&M University

Dr. Henry F. Taylor

APPROVED FOR PUBLIC RELEASE; DISTRIBUTION UNLIMITED.

DTIC
ELECTE
DEC 03 1990
S B D
C

Rome Air Development Center
Air Force Systems Command
Griffiss Air Force Base, NY 13441-5700

This report has been reviewed by the RADC Public Affairs Division (PA) and is releasable to the National Technical Information Services (NTIS) At NTIS it will be releasable to the general public, including foreign nations.

RADC-TR-90-234 has been reviewed and is approved for publication.

APPROVED:



DAVID A. GARAFALO
Project Engineer

APPROVED:



JOHN A. GRANIERO
Technical Director
Directorate of Communications

FOR THE COMMANDER:



BILLY G. OAKS
Directorate of Plans & Programs

If your address has changed or if you wish to be removed from the RADC mailing list, or if the addressee is no longer employed by your organization, please notify RADC (DCLW) Griffiss AFB NY 13441-5700. This will assist us in maintaining a current mailing list.

Do not return copies of this report unless contractual obligations or notices on a specific document require that it be returned.

REPORT DOCUMENTATION PAGE

Form Approved
OMB No. 0704-0188

Public reporting burden for this collection of information is estimated to average 1 hour per response, including the time for reviewing instructions, searching existing data sources, gathering and maintaining the data needed, and completing and reviewing the collection of information. Send comments regarding this burden estimate or any other aspect of this collection of information, including suggestions for reducing this burden, to Washington Headquarters Services, Directorate for Information Operations and Reports, 1215 Jefferson Davis Highway, Suite 1204, Arlington, VA 22202-4302, and to the Office of Management and Budget, Paperwork Reduction Project (0704-0188), Washington, DC 20503.

1. AGENCY USE ONLY (Leave Blank)		2. REPORT DATE September 1990		3. REPORT TYPE AND DATES COVERED Final Feb 89 - Mar 90	
4. TITLE AND SUBTITLE DIRECT OPTICAL TO MICROWAVE CONVERSION				5. FUNDING NUMBERS C - F30602-88-D-0028 PE - 63726F PR - 2863 TA - 92 WU - PH	
6. AUTHOR(S) Dr. Henry F. Taylor					
7. PERFORMING ORGANIZATION NAME(S) AND ADDRESS(ES) Texas A&M University Department of Electrical Engineering College Station TX 77843				8. PERFORMING ORGANIZATION REPORT NUMBER	
9. SPONSORING/MONITORING AGENCY NAME(S) AND ADDRESS(ES) Rome Air Development Center (DCLW) Griffiss AFB NY 13441-5700				10. SPONSORING/MONITORING AGENCY REPORT NUMBER RADC-TR-90-234	
11. SUPPLEMENTARY NOTES RADC Project Engineer: David A. Garafalo/DCLW/(315) 330-3571 The prime contractor for this effort was University of Dayton, Dayton OH 45469-0001.					
12a. DISTRIBUTION/AVAILABILITY STATEMENT Approved for public release; distribution unlimited.				12b. DISTRIBUTION CODE	
13. ABSTRACT (Maximum 200 words) Support of high frequency fiber optic links through development of innovative higher efficiency techniques to convert optical energy directly to RF Energy. <u>OPPORTUNITY</u> : Control of Phased Arrays by optical means is an area of expanding technology development. Fiber optics and other forms of optical waveguide can provide greater accuracy and true time delay in a phase delay network. <u>OBJECTIVE</u> : Determine methods of improvement in transfer of optical energy to RF Energy. <u>CONTRIBUTION</u> : Development of Direct Optical-to-RF-Direct Amplifiers will result in higher efficiency, low noise, optical receivers for fiber optic links with improved performance. This will result in longer fiber optic links without repeaters and improved BER on shorter links.					
14. SUBJECT TERMS Optical to Microwave Conversion				15. NUMBER OF PAGES 36	
				16. PRICE CODE	
17. SECURITY CLASSIFICATION OF REPORT UNCLASSIFIED		18. SECURITY CLASSIFICATION OF THIS PAGE UNCLASSIFIED		19. SECURITY CLASSIFICATION OF ABSTRACT UNCLASSIFIED	
				20. LIMITATION OF ABSTRACT SAR	

TABLE OF CONTENTS

Introduction	1
Objectives	1
Progress	2
Conclusions and Recommendations	9
References	10
Appendix A. "Traveling Wave Photodetectors"	11
Appendix B. "Analysis of Depleted TW Photodetectors"	17



Revision For 101 102 103 104	<input checked="" type="checkbox"/> <input type="checkbox"/> <input type="checkbox"/>
By	
Date	
Available Codes	
Dist	
A-1	

Introduction:

The key to many of the microwave applications of optics will be the ability to integrate photodetectors with monolithic microwave integrated circuits (MMIC's). This will allow microwave signals to be coupled optically into MMICs via fiber optic lines. Such optoelectronic integrated circuits (OEICs) could have widespread application in Air Force electronic warfare and radar systems. Monolithic OEIC technology is in its infancy, and many aspects of device fabrication and application remain to be explored.

Objectives:

Building upon the technology base established at Texas A&M over the past several years, we will explore new possibilities for optically coupled microwave devices. These include a monolithic optoelectronic differential amplifier, a traveling wave (TW) photodetector, and integration of such a photodetector with a microwave field transistor (FET) amplifier.

Optoelectronic Differential Amplifier

Optoelectronic differential amplifiers¹ which operate at much higher bandwidths than conventional electronic operational amplifiers will be constructed. Light from two laser diodes driven by microwave input signals will illuminate two photodetectors on a monolithic balanced receiver chip. Waveforms from the photodetectors will be subtracted in a common load resistor on this chip to produce a differential output. The goal is to show that a monolithic version of the optoelectronic differential amplifier can operate at bandwidths in the 5-10 GHz range. Such a device could be useful for signal processing in electronic warfare and radar systems. The balanced receiver chip could prove effective in coherent communications as well.

Traveling Wave Photodetector

This device will be configured as a coplanar transmission line on a semiinsulating gallium arsenide substrate. Light modulated at microwave frequencies will be coupled into the stripline gap to produce electron-hole pairs. The resulting current flow in the gap will produce a microwave signal on the transmission line. Phase matching of optical and microwave signals will be accomplished with optical delay lines. A configuration in which the incident light is confined in two dimensions by an optical waveguide will also be explored. The TW photodetector will be readily integrable with other microwave elements, and its

distributed nature will allow higher microwave power levels to be generated than with other types of photodetector.

Progress

Optoelectronic Differential Amplifier

Several balanced receivers for the optoelectronic differential amplifier have been fabricated in semiinsulating gallium arsenide and characterized over the frequency range 0 - 8 GHz. These receivers have 3 μm -wide photoconductive gaps to which independent bias voltages of opposite polarity are applied. The photocurrent from the two gaps is subtracted in a common load. The rf characterization is carried out using modulated semiconductor laser diodes. In order to simultaneously excite both gaps, the modulated laser light is coupled into a single mode fiber and passed through a 50:50 coupler to provide two optical outputs of approximately equal amplitude. The light from each of two fibers is imaged into one of the photoconductive gaps. Coupling from each fiber to the corresponding gap can be varied independently using a micromanipulator to position the fiber, to facilitate signal subtraction.

The rf response has been measured for three of the devices as a function of the gap bias voltages laser modulation frequency. Optimum voltage of operation was found to be in the neighborhood of 15 V. Instabilities in the device output due to electromagnetic interference between various elements of the system have been eliminated by improved rf shielding. The common-mode rejection ratio (CMRR) for one of the devices ranged from 16-22 dB over the frequency range from 0.5 - 7.5 GHz. A second device showed CMRR values from 14-25 dB over that same range.

This device can perform at much higher frequencies than conventional electronic differential amplifiers, because in the optoelectronic design the signal inputs are decoupled from the rest of the circuit. This points the way to a new class of optoelectronic signal processors for wideband signals.

These results are described in detail in Ref. 2.

Traveling Wave Photodetector

Fiber optic communication systems suffer an inherently limited optical-to-electrical conversion efficiency. This is a concern when fiber optics are used for analog microwave transmission, because the signal must generally be amplified at the receiver to restore a usable microwave signal level. Since amplification is required even if the length of the fiber cable is very small, this represents a competitive

disadvantage for fiber optics versus conventional microwave transmission media (coaxial cable or metal waveguide).

As a baseline for estimating the degree of amplification needed, we consider a semiconductor pn or Schottky diode photodetector designed for multigigahertz response. Light modulated at a microwave frequency f is incident upon the photodetector. The microwave power P_m delivered into a load resistor R can be written

$$P_m = RI_m^2, \quad (1)$$

where I_m is the root-mean-square (rms) current generated in the photodetector at the frequency f . This current can be related to the detector responsivity r and the modulated rms optical power level P_{opt} by the relation

$$I_m = rP_{opt} \quad (2)$$

For a typical short-distance microwave fiber optics link, we might have $P_{opt} = 1 \text{ mW}$, $R = 50 \Omega$, and $r = 0.6 \text{ A/W}$. Combining (1) and (2), we calculate that $P_m = 1.8 \times 10^{-5} \text{ W} = -17.4 \text{ dBm}$. This means that the optical-to-microwave conversion efficiency ϵ , defined as

$$\epsilon = P_m/P_{opt}, \quad (3)$$

is -17.4 dB . If the optical signal were attenuated by transmission over a longer fiber, such that $P_{opt} = 1 \mu\text{W}$, then we calculate that $P_m = 1.8 \times 10^{-11} \text{ W} = -77.4 \text{ dBm}$ and $\epsilon = -47.4 \text{ dBm}$.

Another important performance parameter of the fiber optic link is the dynamic range relative to the noise, D , defined by the relation

$$D = (P_m)_{max}/P_n, \quad (4)$$

where $(P_m)_{max}$ is the maximum microwave power generated in the receiver and P_n is the receiver noise. Generally thermal noise dominates at microwave frequencies, so we can write

$$P_n = kTBF, \quad (5),$$

where k is Boltzmann's constant ($k = 1.38 \times 10^{-23} \text{ J/}^\circ\text{K}$), T is the absolute temperature in degrees Kelvin, B is the microwave bandwidth, and F is the amplifier noise figure. At room temperature ($T = 293^\circ \text{K}$), for $B = 1 \text{ GHz}$ and $F = 2$ (3 dB), we find that $P_n = 8.1 \times 10^{-12} \text{ W} = -80.9 \text{ dBm}$. In the example above with $P_{opt} = 1 \text{ mW}$, we calculate a dynamic range of 63.5 dB. With an optical power of $1 \mu\text{W}$, the dynamic range is reduced to only 3.5 dB.

Since both the microwave power level and the dynamic range are proportional to the square of the rms microwave photocurrent I_m , it is important to achieve the maximum possible value for I_m . However, in conventional small-area ($\approx 25 \times 25 \mu\text{m}^2$) photodetectors designed for microwave frequencies, the photocurrent saturates at relatively low values ($\approx 10 \text{ mA}$) due to heat dissipation and space-charge effects. A traveling wave photodetector with a coplanar stripline configuration represents a way to overcome these limitations. First, the heat generated by current flow in the photodetector can be distributed over a cm or more of length, providing order-of-magnitude reduction in the temperature rise in the active region of the device. Secondly, the current flow is distributed over a much larger cross-section, so that space-charge effects are correspondingly reduced. A third advantage is the ease of integration with other microwave circuit elements, such as FET amplifiers and Gunn oscillators.

A traveling wave photodetector consisting of a coplanar transmission line on a semiinsulating gallium arsenide substrate has been fabricated in our laboratory and preliminary tests have been completed. Our design uses $3 \mu\text{m}$ gaps and $28 \mu\text{m}$ wide striplines to form a 5 cm long, 50Ω transmission line, as illustrated in Fig. 1. The electrode mask was produced using our in-house laser scanning system. The striplines are about $0.34 \mu\text{m}$ thick and consist of $0.2 \mu\text{m}$ of gold on a Ni-Au/Ge base which is annealed to form ohmic contact with the substrate, as in Fig. 2. Light modulated at microwave frequencies is coupled into the stripline gap to produce electron-hole pairs. The resulting photoconductive current flow produces a microwave signal on the transmission line. Phase matching of the optical and microwave signals is accomplished with an optical delay line arrangement, as in Fig. 3.

Some initial results showing the microwave interference between two optical input signals injected at different locations on the transmission line are shown in Fig. 4. These measurements were made with a directly modulated Ortel laser diode as the light source. The modulated optical power was maintained at a low value ($\approx 10 \mu\text{W}$) to avoid the risk of damaging the laser diode. The maximum optical power generated in these preliminary measurements over the $0.2\text{-}3.5 \text{ GHz}$ range was -81 dBm . When optical losses in the measurement system (Fig. 3) are taken into account, the value of P_{opt} (eq. 2) is about $1 \mu\text{W}$, giving an optical-to-microwave conversion efficiency of about -51 dB . These initial results are encouraging in that they demonstrate the interference effect in a traveling wave structure, but considerable improvement in conversion efficiency as well as monolithic integration of the TW photodetector with an amplifier will be needed before such an approach can prove practical for radar system application.

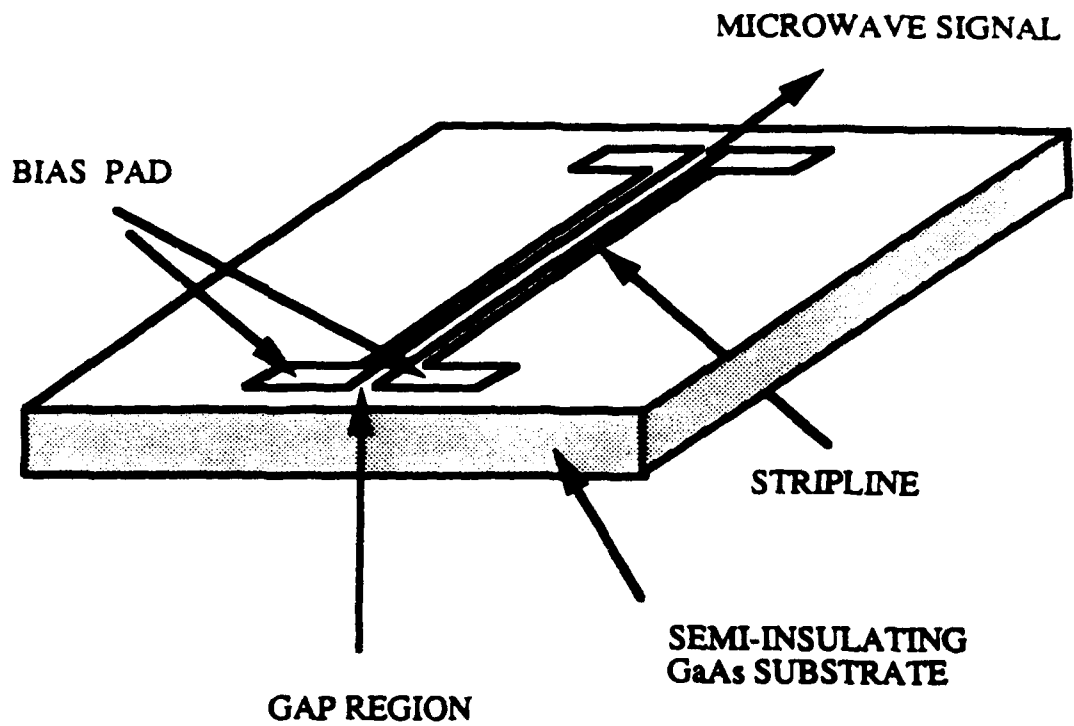
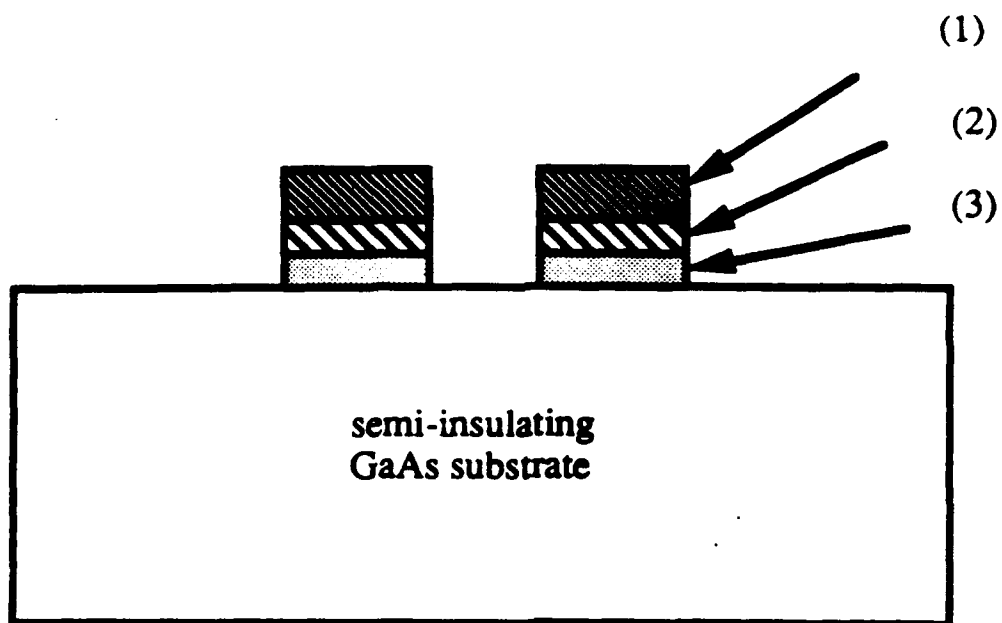


Fig. 1. Configuration for Traveling Wave Photodetector.



- (1) Au layer : 2000 Å
- (2) Au-Ge layer : 1215Å
- (3) Ni layer : 150 Å

Fig. 2. Electrode Design for TW Photodetector.

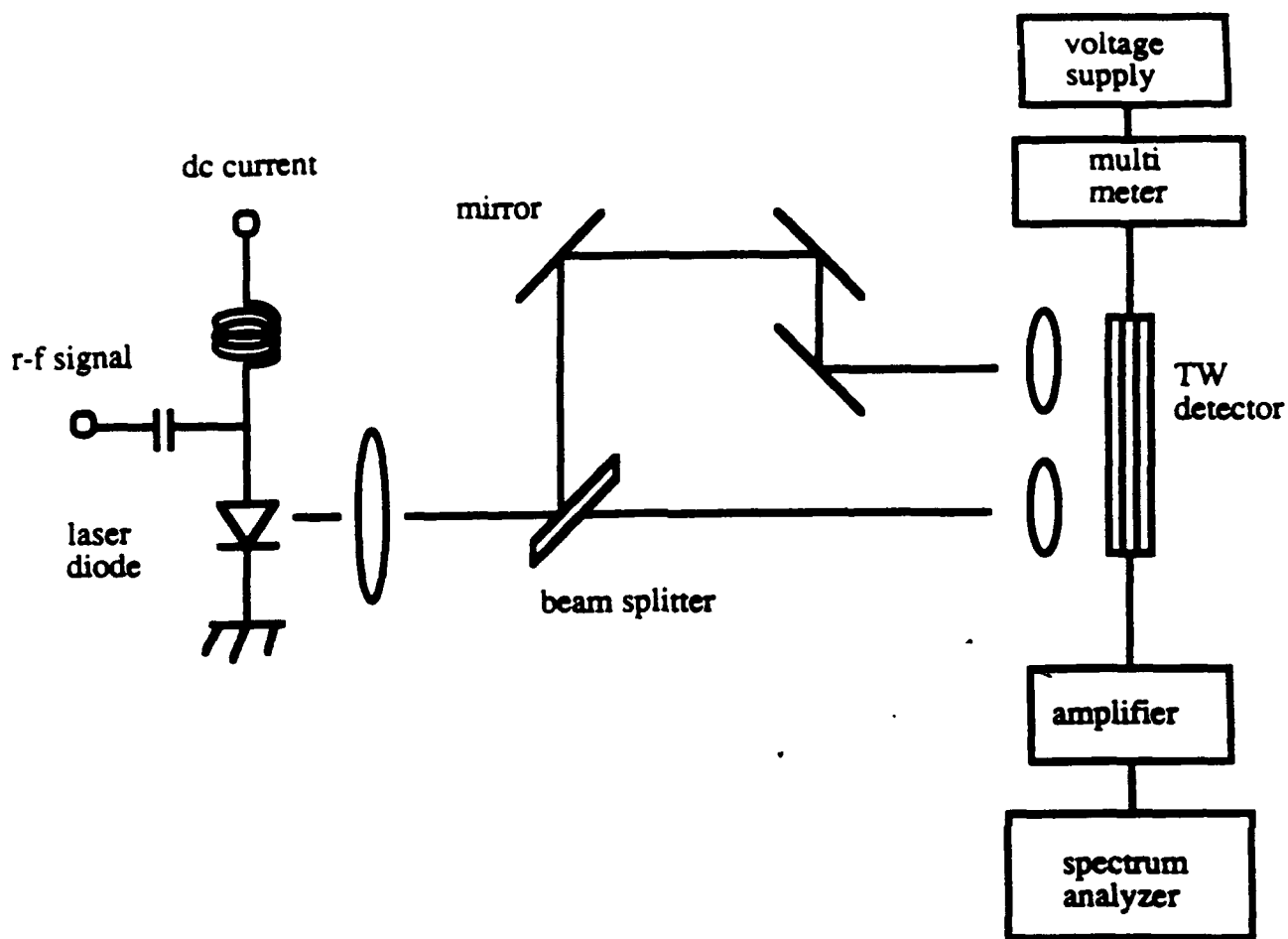


Fig. 3. Setup for Testing TW Photodetector with Two Optical Inputs.

Interference effect due to two input spots

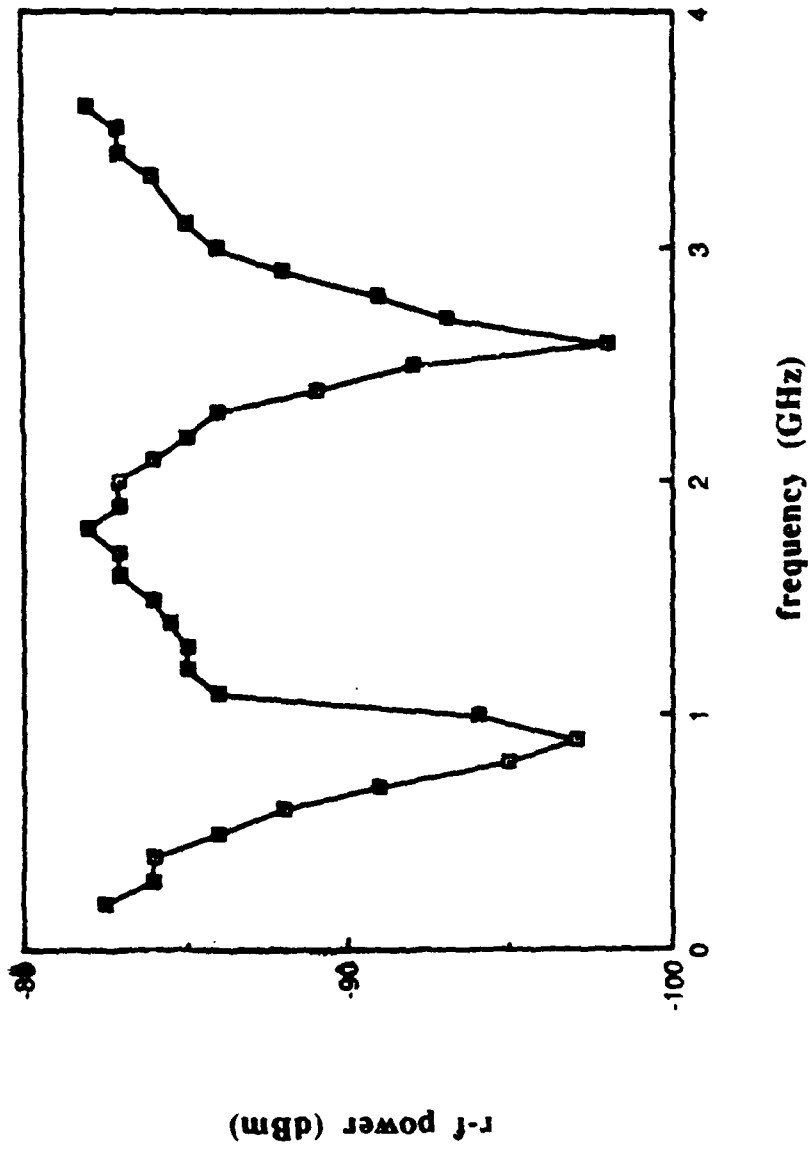


Fig. 4. Experimental Results Showing Microwave Interference Between Two Inputs in TW Photodetector.

A second structure under investigation makes use of an optical waveguide formed in GaAlAs epitaxial layers on a semiinsulating GaAs substrate. The epitaxial layers have been grown for us by Dr. Y. C. Kao of Texas Instruments. A rib waveguide 6 μm wide is formed in the layered sample by reactive ion etching. A coplanar stripline formed on the surface of the sample makes ohmic contact with the top epitaxial layer (GaAs, 0.2 μm thick), which strongly absorbs light at our laser wavelength of 0.83 μm . When modulated light from this laser is coupled into the waveguide, electron-hole pairs are created in this layer as the light propagates down the waveguide. This provides a traveling wave excitation of the transmission line at the modulation frequency. Strong optical waveguiding and a photoconductive effect has been observed in one of the devices. However, the optical absorption was too low in the initial device to obtain meaningful results at microwave frequencies. The device structure is being redesigned for enhanced microwave response.

The TW detectors studied to date under this program have used photoconductivity as the optical-to-microwave transduction mechanism. However, carrier lifetime limits the speed of photoconductive devices with near-unity quantum efficiency to about 10-15 GHz. For performance in the millimeter-wave regime (30 - 300 GHz), a depleted structure (pn junction or Schottky diode) is needed. Design considerations are considerably different than for photoconductive TW detectors. For example, in the junction devices the junction capacitance per unit length is the critical factor in determining transmission line impedance.

Some considerations in the design of TW photodetectors³ are discussed in Appendix A of this report. An analysis of depleted TW photodetector designs is included as Appendix B of this report.

Conclusions and Recommendations

As the results with the optoelectronic differential amplifier indicate, OEICs can provide performance in microwave signal processing which cannot be achieved using only electronic/microwave components. The performance to 8 GHz demonstrated in the optoelectronic device compares with about 200 MHz in the fastest all-electronic differential amplifiers. The TW photodetector also shows promise for optical generation of greater microwave power levels than can be achieved with conventional photodetectors.

It is recommended that the experimental evaluation of the two alternative traveling wave photodetector structures described above be completed over the 2-12 GHz frequency range, and that the more promising of these structures be

selected for integration with an amplifier to provide enhanced optical-to-microwave conversion efficiency. Either of these traveling wave photodetector designs is suitable for integration with a microwave field-effect transistor (FET) amplifier. For example, one of the electrodes can form the gate and the other the drain of the FET. The source and drain of the FET can provide a coplanar line for transmitting the amplified microwave output.

It is also recommended that TW photodetectors based upon pn junction or Schottky diode structures be fabricated in suitable epitaxial material on semiinsulating GaAs substrates. Such structures offer the best prospect for millimeter-wave response in OEIC devices.

Finally, it is recommended that a setup for generating a beat frequency from two high-power laser diodes be assembled and used in future evaluation of the TW photodetectors. With such an arrangement, it should be possible to obtain effective modulated optical power levels of several mW and to demonstrate greatly improved optical-to-microwave conversion efficiencies and dynamic range.

References:

1. Y. A. Choi and H. F. Taylor, "Gigahertz-Bandwidth Optoelectronic Differential Amplifier," *Microwave and Optical Technology Letters*, vol. 1, pp. 49-51, April 1988.
2. K. N. Choi, "Fabrication of Wideband Optoelectronic Differential Amplifier using a Balanced Receiver on a Semiinsulating GaAs Substrate," M. S. Thesis, Texas A&M University, December 1989.
3. H. F. Taylor, O. Eknoyan, C. S. Park, K. N. Choi, and K. Chang, "Traveling Wave Photodetectors," *Society of Photooptical Instrumentation Engineers*, Los Angeles, January 1990.

Appendix A

"Traveling Wave Photodetectors"

Paper presented at SPIE meeting, Los Angeles, January 1990.

Traveling Wave Photodetectors

H. F. Taylor, O. Eknoyan, C. S. Park,
K. N. Choi, and K. Chang

Department of Electrical Engineering
Texas A&M University
College Station, Texas 77843

ABSTRACT

Designs for traveling wave photodetectors in semiconductor materials are presented, and advantages over conventional photodetectors are discussed.

1. INTRODUCTION

Lumped-element designs are used in today's high-speed photodetectors for optical communications and signal processing^{1,2}. The response speed in these devices is limited by the RC time constant, where R is the load impedance and C is the capacitance. In order to maintain very low ($\ll 1$ pf) capacitance values in these devices, it is necessary for the active area to be very small ($\ll 10^{-4}$ cm²). The small area can be a disadvantage in some microwave applications, particularly when it is desired to generate significant power levels at multi-GHz frequencies. The traveling wave (TW) photodetector configuration is proposed as a means of overcoming this limitation.

In a TW photodetector, optical excitation occurs in distributed fashion along the length of a transmission line structure, as illustrated in Fig. 1. It is envisioned that practical TW photodetectors will be fabricated in semiconductor materials such as GaAs or InGaAs. The carrier concentration between electrodes of the transmission line varies with time in response to the modulated optical input signal. A microwave signal is generated on the transmission line as a result of the temporal variation in gap conductivity. Phase matching of the optical and microwave signals is desirable, as the transmission line length for efficient optical-microwave conversion is limited by the degree to which phase matching is achieved.

2. RATIONALE FOR THE TRAVELING WAVE PHOTODETECTOR

There are several reasons that TW photodetector designs might be desirable in some applications. The gap region can be much larger in area than in conventional photodetectors, so that

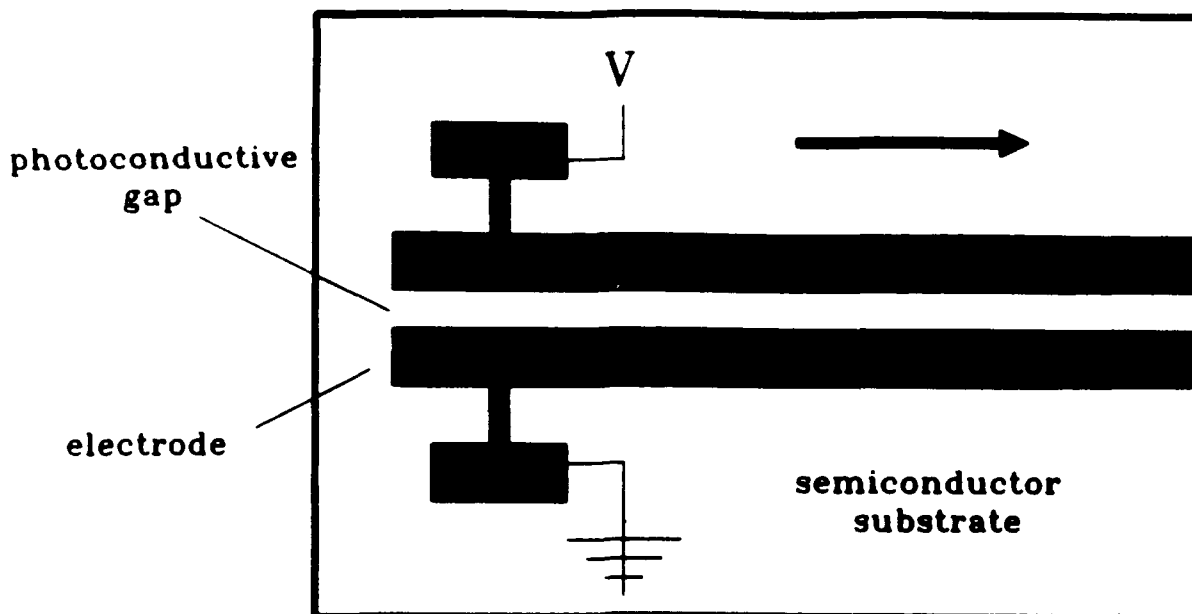


Fig. 1 Coplanar transmission line configuration for a TW photodetector

larger microwave powers can be generated before saturation occurs and before substrate heating reaches excessive levels. Since the photodetector has a transmission line structure, it readily interfaces with other microwave circuit elements. For example, in a coplanar transmission line configuration the two electrodes of the photodetector might easily connect to the drain and gate electrodes of a field-effect transistor (FET) amplifier. Designs for the TW photodetector which employ an optical waveguide are not subject to the quantum-efficiency/speed tradeoff which occurs in conventional photodetectors because of the finite carrier saturation velocity. Finally, some interesting nonlinear optical/microwave effects might be possible with TW photodetector designs.

3. TW PHOTODETECTOR DESCRIPTION

Two approaches to the TW photodetector are discussed here: one in which the light is coupled into the active (photosensitive) region from above, and the other in which an optical waveguide is used for the coupling.

The first approach is illustrated in Fig. 2. The light can be coupled into the gap using cylindrical optics, as in Fig. 2(a), or using optical fibers, as in Fig. 2(b). In either case, phase matching is a primary consideration. For a coplanar line, as in Fig. 1, the phase velocity of the microwave signal v_m is given by

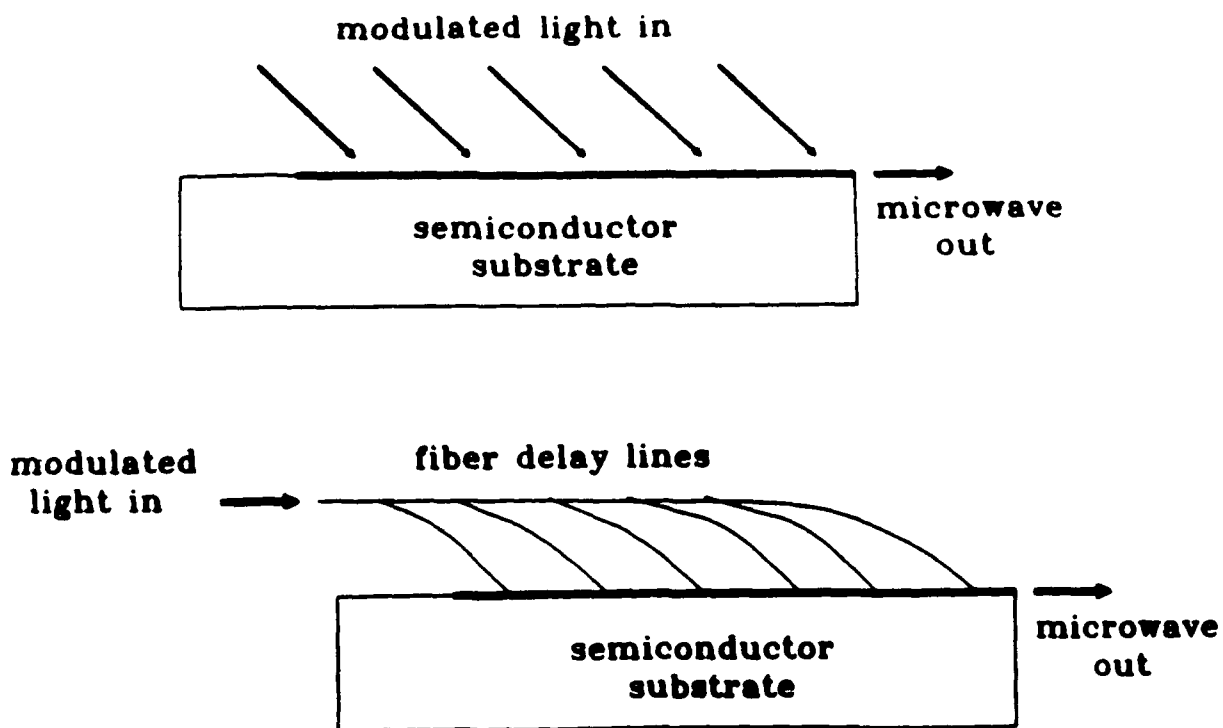


Fig. 2 Phase matching in a TW photodetector

$$v_m = \frac{2^{1/2}c}{(\epsilon/\epsilon_0+1)^{1/2}} \quad (1)$$

with c the free-space velocity of light, ϵ_0 the dielectric permittivity of free space, and ϵ the dielectric permittivity of the substrate. In GaAs, for example, with $\epsilon/\epsilon_0 \approx 13$, $v_m \approx .38 c$. Phase matching for the configuration of Fig. 2(a) with the light incident in air thus requires that $\theta = \sin^{-1}.38 = 22^\circ$, where θ is the angle of the incident light beam relative to the normal to the surface of the substrate. For the configuration of Fig. 2(b), the lengths of the fiber delay lines must be properly adjusted to insure phase matching.

The second approach to the traveling wave photodetector makes use of an optical waveguide to transmit the incident light, as in Fig. 3. An optically absorbing region is provided as a part of the waveguide structure so that photogenerated carriers are produced in the stripline gap. In this case the optical group velocity v_o should be equal to v_m for perfect phase matching, with $v_o = c/n_g$ and n_g the group refractive index of the waveguide mode. In GaAs, for example, with $n_g \approx 4$ near the band edge, $v_o \approx .25 c \approx .66 v_m$. To achieve better phase matching, a dielectric overlay could be provided on top of the transmission line. In fact, if the transmission line of Fig. 1 were buried in GaAs the value of v_m would be reduced to $.27 c$, so that almost perfect phase matching would be achieved.

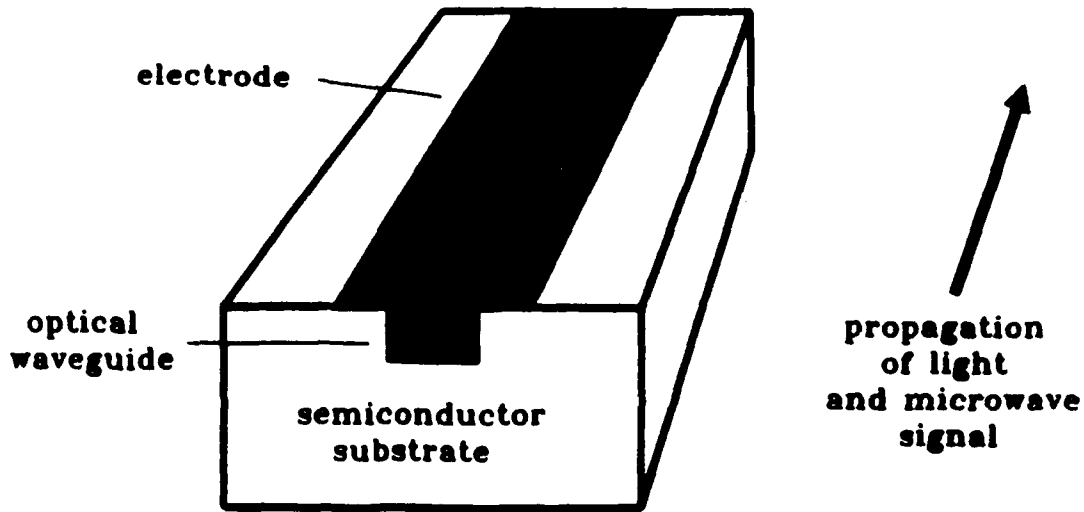


Fig 3. Optical waveguide configuration for TW photodetector.

An optical waveguide structure for the TW photodetector in the AlGaAs alloy system is illustrated in Fig. 4. This design could be used for detection of AlGaAs laser emission at wavelengths in the vicinity of $.83 \mu\text{m}$. The top GaAs layer and the adjacent AlGaAs layer serve as the optical waveguide. The next AlGaAs layer serves as a buffer to provide optical isolation of the light from the substrate. Lateral confinement of the light is provided by the mesa etched into the top layer. Light propagating in the waveguide is absorbed in the top layer, which has a smaller band gap than the laser photon energy, and produces a photoconductive current between the electrodes. The electrodes are in ohmic contact with the photoconductive layer.

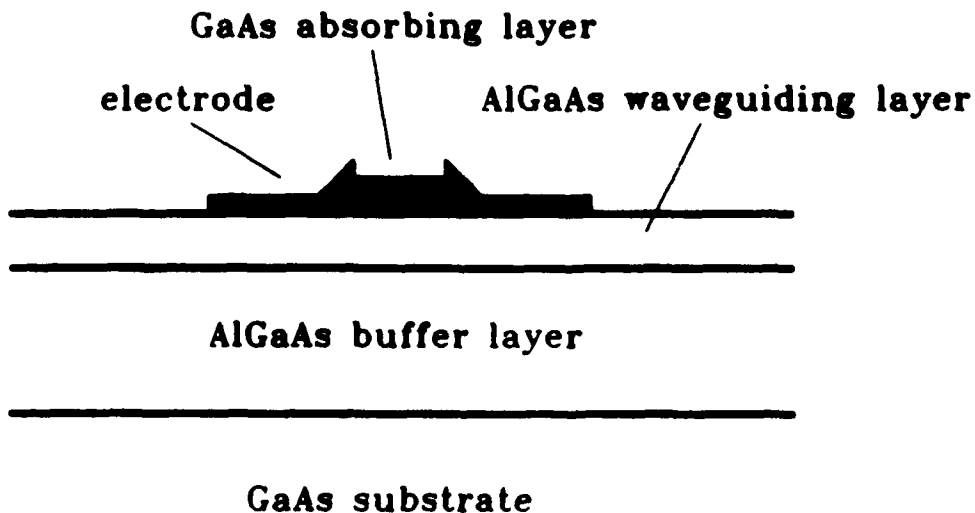


Fig. 4 TW photodetector in AlGaAs.

4. IDEAL TW PHOTODETECTOR DESIGN

A number of desirable features of the TW photodetector can be identified. The quantum efficiency for conversion of photons to electron-hole pairs should be near unity. Although photoconductive detectors can perform well at frequencies to 10 GHz and beyond, for most microwave applications depleted structures (pn junction or Schottky barrier) are preferred. With depletion regions of the order of 0.3 μm thick, performance can extend to 100 GHz. Avalanche gain might be incorporated as a means of enhancing the microwave power generation, but at the cost of reduced speed and higher noise levels. A 50 Ω impedance is desired in order to easily interface the TW photodetector with off-chip transmission lines. Finally, simple fabrication is desirable.

5. CONCLUSIONS

Traveling wave photodetectors would appear to have promise for use in microwave transmission systems. They should be easy to interface with other monolithic microwave integrated circuit (MMIC) components. Higher optically generated microwave power levels should be possible than with conventional photodetectors. Optical waveguide coupling would appear to offer the possibility of achieving both high quantum efficiency and high speed. Finally, some interesting possibilities may exist for nonlinear optical-microwave interactions in structures similar to those described in this paper.

6. REFERENCES

1. D. H. Newman and S. Ritchie, "Sources and Detectors for Optical Fiber Communication Applications: The First 20 Years," IEE Proceedings, Part J, pp. 213-229, June 1986.
2. M. Brain and T. P. Lee, "Optical Receivers for Lightwave Systems," IEEE Journal of Lightwave Technology, vol. LT-3, pp. 1281-1300, December 1985.

Appendix B

"Design of Depleted TW Photodetectors"

prepared by

B. Kwark

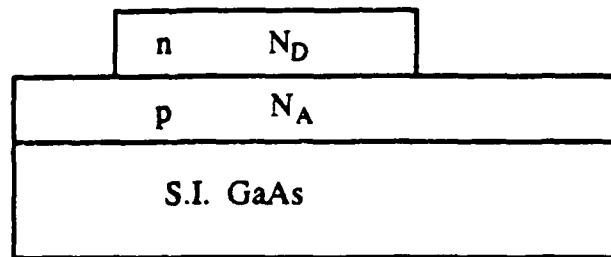
Texas A&M University

March 1990

1. Epi-layer Design Consideration

This section includes some important parameters which must be considered to design the structure of PN traveling wave detector.

For high-speed operation, the depletion region must be kept thin to reduce the transit time. On the other hand, to increase the quantum efficiency, the depletion layer must be thick to allow a large fraction of the incident light to be absorbed. Thus there is a trade-off between the speed of response and quantum efficiency. Here is schematic diagram for depletion layer thickness consideration.



N_D : to be decided

N_A : 1.0×10^{18}

Φ_0 : contact internal potential

ϵ_r : 13.6

V : reverse bias voltage

E : electric field over depletion region

$$\Phi_0 = \frac{kT}{e} \ln \frac{N_D N_A}{n_i^2}$$

$$D = \left[\frac{2\epsilon_0 \epsilon_r}{e} (\Phi_0 - V) \left(\frac{1}{N_D} + \frac{1}{N_A} \right) \right]^{\frac{1}{2}}$$

$$E = \frac{\Phi_0 - V}{D}$$

$$V \leq 0$$

As rule of thumb, the depletion layer should be created as close to the surface as possible for efficiency. This can be realized by making low doped n-layer on high doped p-layer, in which structure large portion of depletion layer can be created in n-layer side only. Another key factor for better quantum efficiency is the absorption coefficient. To allow that most light will be absorbed in depletion region, the depletion region must be of the order of $1/\alpha$. At GaAs wavelength, $0.83\mu\text{m}$, absorption coefficient, α , is about $7.0 \times 10^3 \text{ cm}^{-1}$, resulting in $1/\alpha \approx 1.5 \mu\text{m}$. The last key is transit time. Because of the limitation of transit time effect depletion region should not be too wide. The optimum compromise occurs when the depletion layer is chosen so that the transit time is of the order of one-half the modulation period.

$$\tau_d = \frac{1}{2f}$$

$$= \frac{D}{v_s}$$

Assuming $v_s = 1.0 \times 10^7 \text{ cm/s}$, $D = 50/f$ (μm) for f in GHz. Couple of D corresponding to various modulation frequency are shown below.

200 GHz	-----	0.25 μm
100 GHz	-----	0.5 μm
50 GHz	-----	1.0 μm

As conclusion depletion region should be in range from 0.25 to 1.5 μm by adjusting external reverse bias voltage. D , depletion region, as function of V for different N_D is shown in Fig. 1. Also electric field is shown as a function of V in Fig. 2. Within range of 0.25 ~ 1.5 μm depletion layer the corresponding electric field is approximately $1.0 \times 10^7 \text{ cm/s}$ by Fig. 3.

As a result the optimum N_D seems to be $2.0 \times 10^{16} / \text{cm}^3$.

Fig. 1. depletion layer thickness

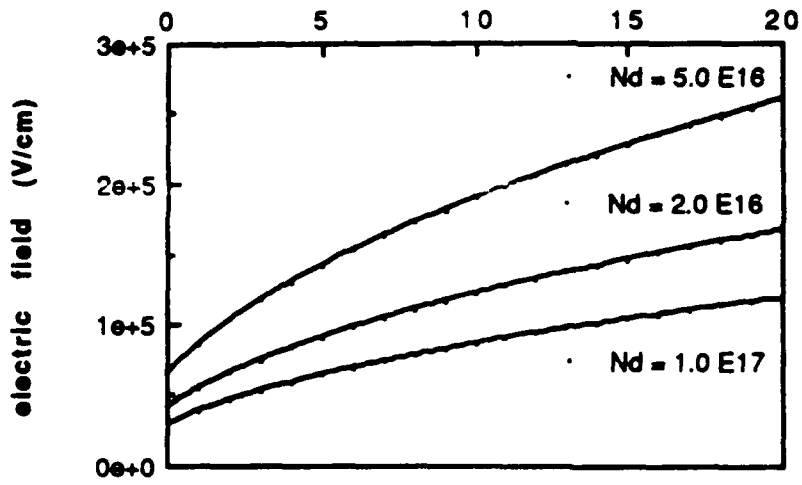
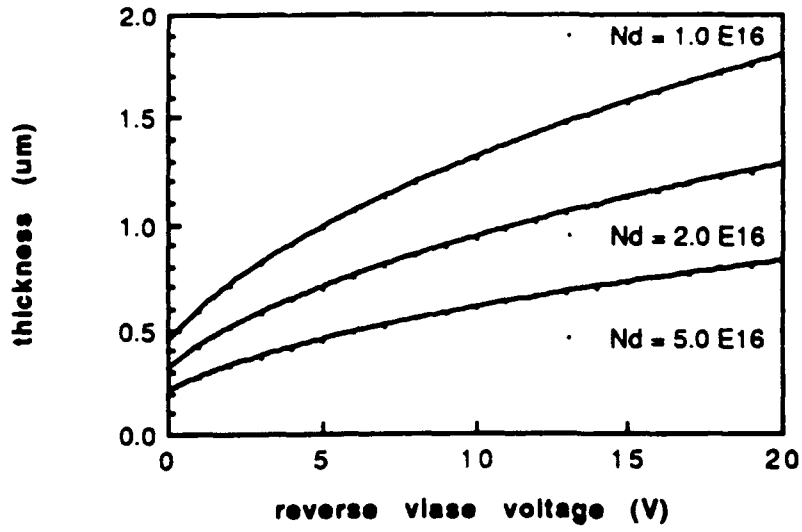


Fig. 2. Electric field

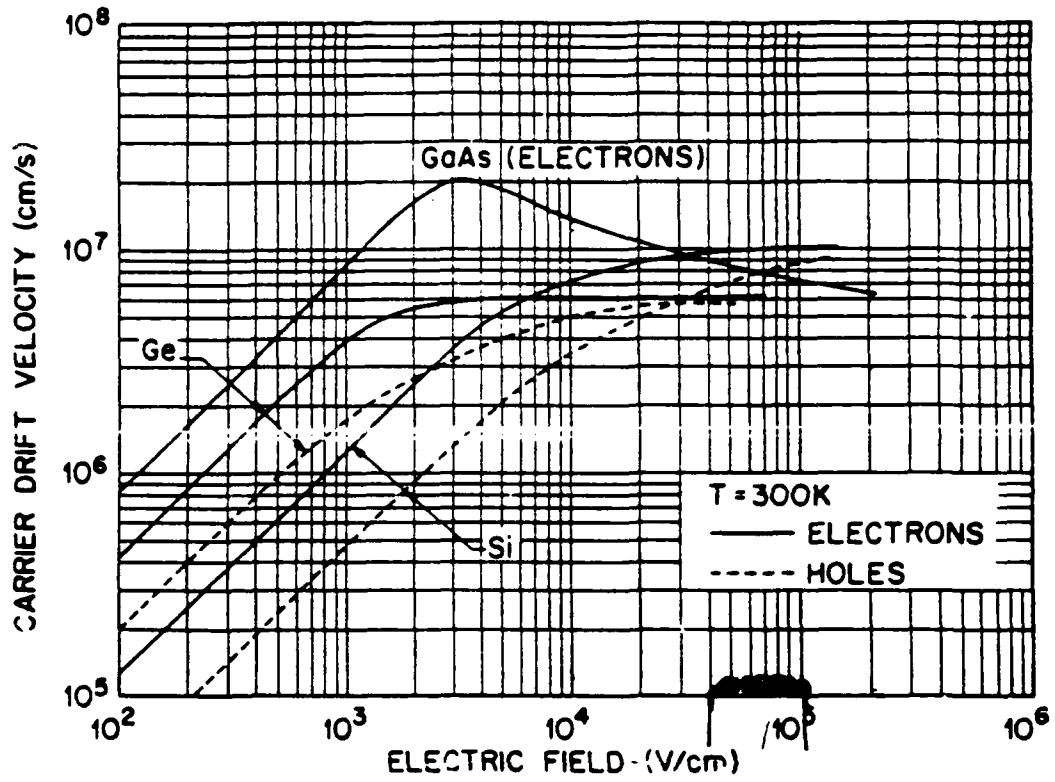


Fig. 3. Carrier drift velocity

2. Vertical Structure of Device



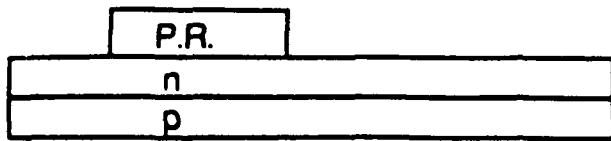
Assuming the range of operation frequency is between 2 ~ 200 GHz, the thickness of n-layer is chosen as 1 μm by previous discussion.

P-layer thickness is not so important as that of n-layer and chosen as 3 μm .

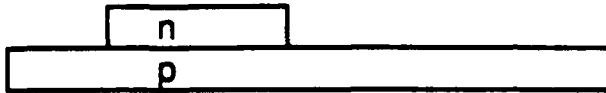
For ohmic contact metal has Gold-Germanium:Nickel:Gold structure.

For the better performance AR coating can be added on n-layer.

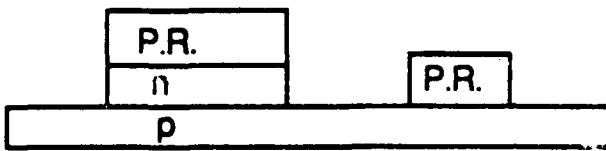
In following page fabrication procedure for this device is suggested.
This process needs three masks.



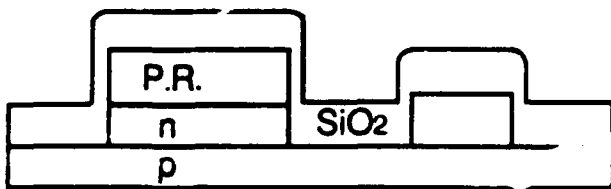
P.R. Pattern



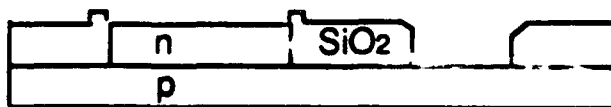
Etch n-layer



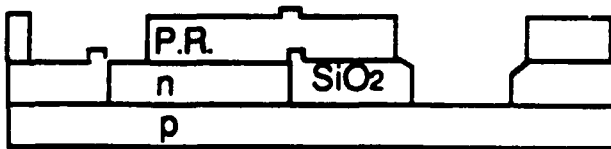
P.R. Pattern



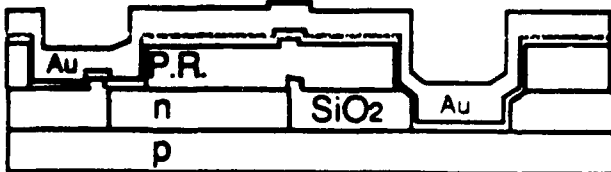
Dielectric Growth
(SiO₂ or Si₃N₄)



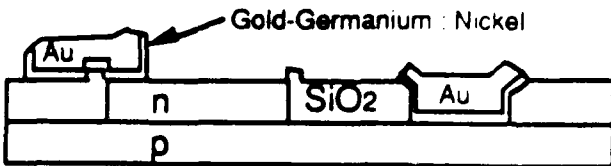
Lift-off



P.R. Pattern

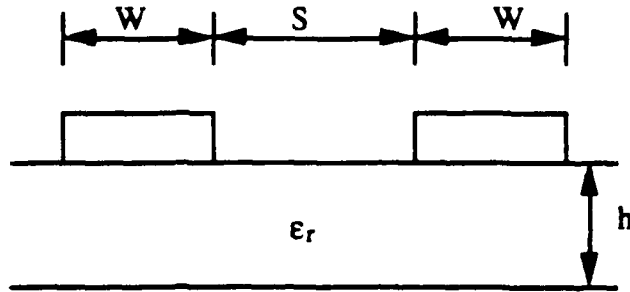


Metal Layer
Gold
Nickel
Gold-Germanium



3. Lateral Structure with Impedance Matching

Assuming coplanar striplines on plain S.I. GaAs substrate without any topology, following equations are used for impedance matching.



$$Z_0 = \frac{120 \pi}{\sqrt{\epsilon_e}} \frac{K(k)}{K(k')}$$

$$\epsilon_e = 1 + \frac{\epsilon_r - 1}{2} \frac{K(k')}{K(k)} \frac{K(k_1)}{K(k_1')}$$

$$k = \frac{a}{b}, \quad a = \frac{S}{2}, \quad b = \frac{S + 2W}{2}$$

$$k_1 = \frac{\sinh\left(\frac{\pi a}{2h}\right)}{\sinh\left(\frac{\pi b}{2h}\right)}$$

$$\frac{K(k)}{K(k')} = \begin{cases} \left[\frac{1}{\pi} \ln \left(2 \frac{1 + \sqrt{k'}}{1 - \sqrt{k'}} \right) \right]^{-1} & 0 \leq k \leq 0.7 \\ \frac{1}{\pi} \ln \left(2 \frac{1 + \sqrt{k}}{1 - \sqrt{k}} \right) & 0.7 \leq k \leq 1 \end{cases}$$

Fig.5 shows width as function of S to meet 50Ω impedance matching. This configuration is not easy to meet. Hence here propose approximate stripline pattern which has $1.0 \times 1.0 \mu\text{m}^2$ pads and $10 \mu\text{m}$ separation between $100 \mu\text{m}$ striplines in active region.

Fig. 5. W vs. S for 50Ω impedance

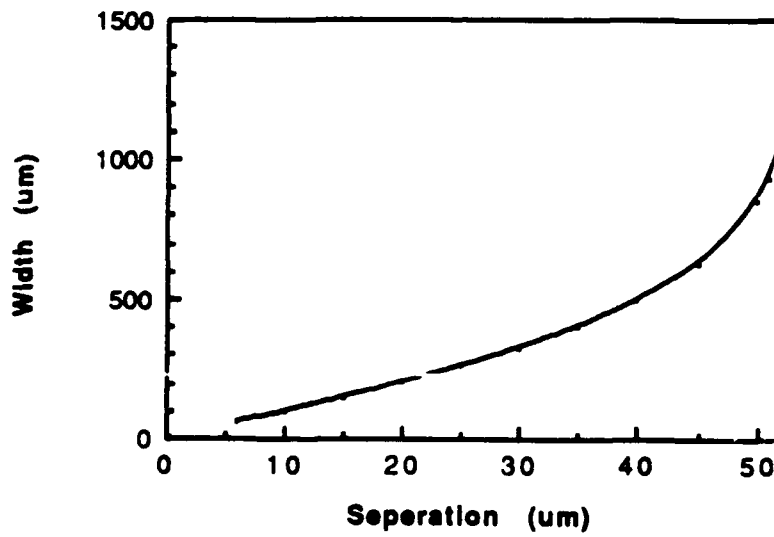


Fig. 6. Stripline Pattern

